APS physics

CHORUS

This is the accepted manuscript made available via CHORUS. The article has been published as:

Quantum interference in the field ionization of Rydberg atoms

Rachel Feynman, Jacob Hollingsworth, Michael Vennettilli, Tamas Budner, Ryan Zmiewski, Donald P. Fahey, Thomas J. Carroll, and Michael W. Noel

Phys. Rev. A **92**, 043412 — Published 13 October 2015

DOI: 10.1103/PhysRevA.92.043412

Quantum Interference in the Field Ionization of Rydberg Atoms

Rachel Feynman,[1] Jacob Hollingsworth,[2] Michael Vennettilli,[2] Tamas Budner,[2]
Ryan Zmiewski,[2] Donald P. Fahey,[1] Thomas J. Carroll,[2] and Michael W. Noel[1]

[1]*Department of Physics, Bryn Mawr College, Bryn Mawr, PA 19010.*
[2]*Department of Physics and Astronomy, Ursinus College, Collegeville, PA 19426.*

We excite ultracold rubidium atoms in a magneto-optical trap to a coherent superposition of the three $|m_j|$ sublevels of the $37d_{5/2}$ Rydberg state. After some delay, during which the relative phases of the superposition components can evolve, we apply an electric field pulse to ionize the Rydberg electron and send it to a detector. The electron traverses many avoided crossings in the Stark levels as it ionizes. The net effect of the transitions at these crossings is to mix the amplitudes of the initial superposition into the same final states at ionization. Similar to a Mach-Zehnder interferometer, the three initial superposition components have multiple paths by which they can arrive at ionization and, since the phases of those paths differ, we observe quantum beats as a function of the delay time between excitation and initiation of the ionization pulse. We present a fully quantum mechanical calculation of the electron's path to ionization and the resulting interference pattern.

PACS numbers: 32.80.Ee, 32.60.+i

I. INTRODUCTION

Because the valence electron in a Rydberg atom is only weakly bound to the core, its energy levels are easily shifted by the Stark effect with modest electric fields. The resulting rich behavior of Rydberg atoms in electric fields has been exploited for a wide range of experiments. Recently, Rydberg atoms have been developed as sensors to measure microwave electric fields with results superior to traditional methods [1, 2]. The Rydberg electron wave function is easily perturbed by the image charge produced in a nearby metal surface and hence Rydberg atoms have been used as a sensitive probe of atom-surface interactions [3] and to measure electric fields near the surface of atom chips [4].

The ionization of Rydberg atoms has been studied in some depth, providing insight into quantum dynamics in an atomic system over vastly different timescales. In the terahertz regime the impulsive energy transfer of a fast half cycle pulse has been used to study wave packet dynamics [5]. Ionization of low lying Rydberg states with single cycle terahertz pulses has revealed an unexpected n^{-3} scaling of the field ionization threshold [6]. Multiphoton ionization with microwave fields has provided insight into the connection between a field and photon picture of the electron's pathway to freedom [7]. In the case where the microwave frequency is close to that of the classical Kepler frequency a variety of interesting behaviors have been observed including resonances in the ionization spectrum [8, 9], population of extremely highly excited states [10, 11], and a phase dependent threshold for ionization of a wavepacket [12, 13]. On the microsecond timescale, the widely used technique of state selective field ionization relies on the relative ease with which the electron can be liberated with a simple and reproducible electric field pulse [14]. It is the ionization of Rydberg atoms with a slowly rising electric field pulse that we study in this paper.

The Stark effect mixes energy levels of the same magnetic quantum number and produces a complex set of many avoided crossings [15]. An example of a Stark map can be seen in Fig. 1 and an idealized two state avoided crossing is shown in Fig. 2. As the electric field is changed, amplitude in one state can transfer to the other state at an avoided crossing. The Landau-Zener-Stückelberg-Majorana (LZ) formula can be used to calculate the probability of a diabatic transition for an ideal two state avoided crossing [16–19].

The LZ transitions that occur at avoided crossings are useful for quantum control and interferometry. In solid state physics, LZ transitions have been used as a beamsplitter for manipulating a superconducting qubit with Mach-Zehnder interferometry [20], for coherent control of a qubit system [21], and again as a beamsplitter for electronic spin states [22]. They have been used to develop quantum memory in diamond nitrogen-vacancy centers [23]. The interference of geometric phase has been observed in a superconducting qubit using LZ interferometry [24]. In atomic physics, chirped microwave pulses have been used to drive LZ transitions between Rydberg states [25–27]. LZ transitions have been observed in a supersonic atomic beam between Rydberg atom pair states [28] and have also been used to manipulate the field ionization spectra of Rydberg atoms by using a shaped field ramp to enhance state selectivity [29, 30].

A Rydberg electron in some initial state can be ionized by applying a time-dependent increasing electric field. The electron's path to ionization depends on the slew rate of the electric field and the characteristics of the avoided crossings [31]. In general, the electron's amplitude will spread over many states due to transitions at the avoided crossings and thus begin to significantly couple to continuum states at multiple different fields. The resulting field ionization spectra have been calculated successfully using multi-channel Landau-Zener theory [32] and a fully quantum mechanical time evolution [33].

Leuchs and Walther observed quantum beats in the

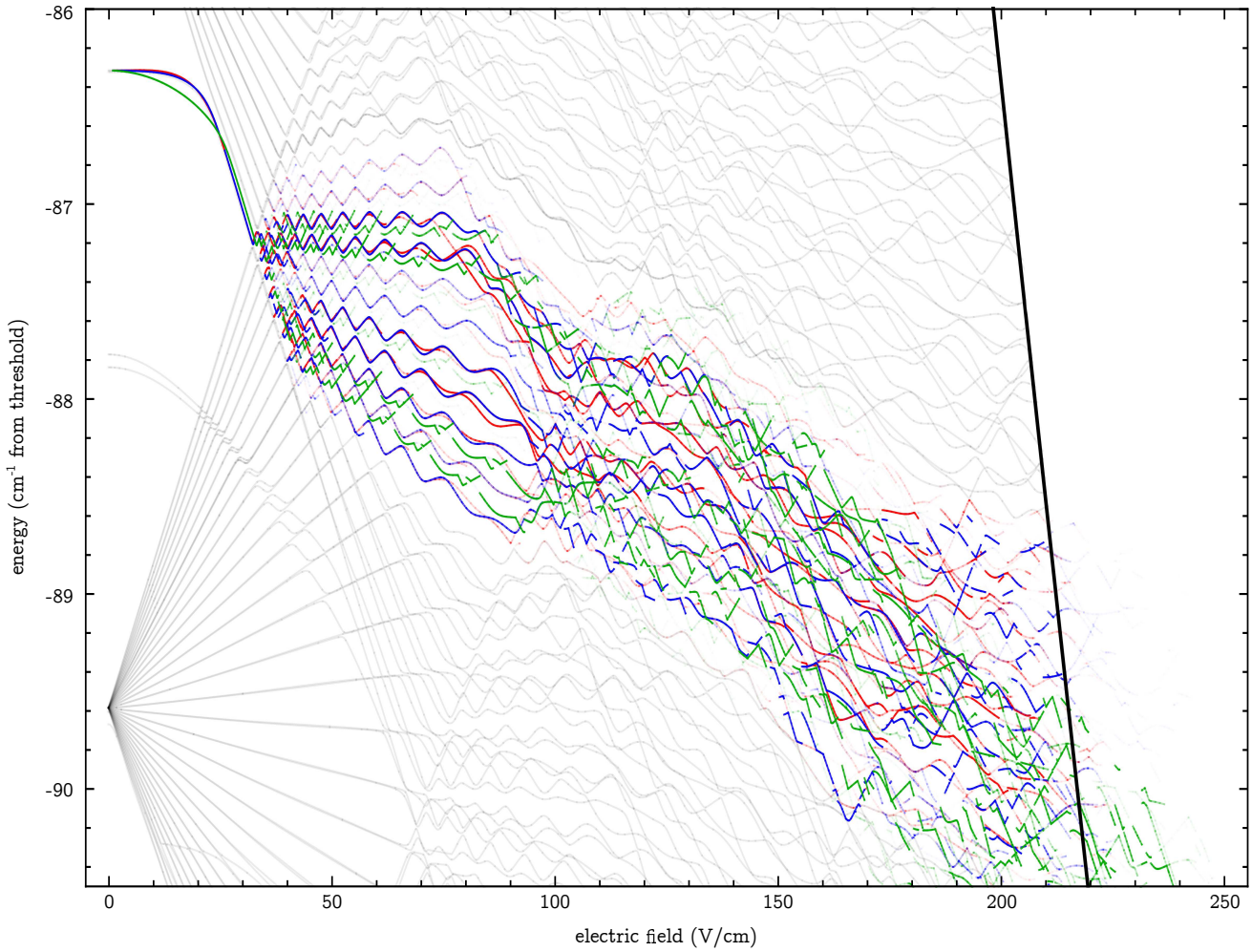

FIG. 1. (color online) Stark map showing the path to ionization for the $37d_{5/2}, |m_j| = 1/2$ (red), the $37d_{5/2}, |m_j| = 3/2$ (blue), and $37d_{5/2}, |m_j| = 5/2$ (green) states. The opacity of the lines is determined by the population in the state for populations less than 0.1. Populations greater than 0.1 are completely opaque. The classical ionization threshold is shown by the thick black line extending upward from about 220 V/cm. The gray background lines are the full $|m_j| = 1/2$ Stark map; they have been terminated at the classical ionization threshold to more clearly display the ionization behavior of the populated states. The green $|m_j| = 5/2$ lines continue well beyond the red $|m_j| = 1/2$ and blue $|m_j| = 3/2$ lines, which is evident in the field ionization spectra shown in Fig. 4.

field ionization spectra of sodium Rydberg atoms due to the energy difference between the fine structure levels [34]. They attributed the quantum beat signal to the interference of the multiple paths through the avoided crossings by which the electron could arrive at the detector. Jeys et al. used quantum beat measurements to explore the behavior of fine structure superposition states as they evolved from low field to the ionization field [35]. We observe similar quantum beats between the magnetic sublevels of the fine structure of rubidium Rydberg atoms. We performed a fully quantum mechanical calculation, similar to that of Førre and Hansen [33], of the path to ionization which preserves all phase information. The $37d_{5/2}$ state of rubidium-85 was selected for the experiments and calculations presented here.

The observed quantum beats can be understood by analogy to a Mach-Zehnder interferometer. A model of the experiment is shown in Fig. 2 which represents a greatly simplified version of a Stark map, showing the energy levels of the Rydberg atom as a function of electric field. The many avoided crossings that the electron will traverse on the way to ionization have been condensed to one representative crossing. A simple example to consider is a superposition of only the $|m_j| = 1/2$ and $|m_j| = 3/2$ states, denoted by $|1/2\rangle$ and $|3/2\rangle$.

The short laser pulse that excites the initial superposition is analogous to the first beamsplitter in a Mach-Zehnder interferometer. The variable time delay before the firing of the ionization pulse allows the phases of the two amplitudes in the superposition to evolve due to the energy difference δ between $|1/2\rangle$ and $|3/2\rangle$; this is analogous to the path length difference in a Mach-Zehnder

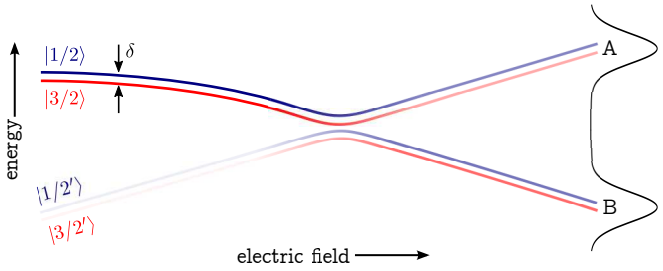

FIG. 2. (color online) A simplified picture of the experiment. Rydberg atoms are excited to coherent superpositions of $||m_j| = 1/2\rangle$ (blue) and $||m_j| = 3/2\rangle$ (red) which have an energy separation of δ. The many avoided crossings that the electron traverses have been condensed into just two avoided crossings with the $||m_j| = 1/2\rangle'$ (blue) and $||m_j| = 3/2\rangle'$ (red) states. The population in each line is shown by the intensity of the color. The relative phase δt between the superposition components is allowed to evolve before an electric field pulse is applied to ionize the electron. As the electric field ramps through the avoided crossing, each component of the initial superposition splits into an adiabatic and a diabatic path. The adiabatic paths ionize together and arrive at the detector at peak **A**. Similarly, the diabatic paths ionize together and arrive at peak **B**. Since the amplitudes from each adiabatic (diabatic) component have a phase difference of δt, quantum beats are observed.

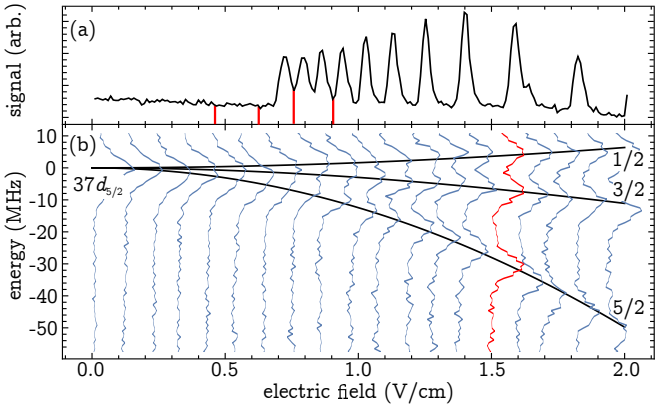

FIG. 3. (color online) (a) Dipole-dipole interaction spectrum for $37d_{5/2}$+$37d_{5/2} \rightarrow 39p$+($n = 35$ manifold), which was used both as an electric field calibration and to pick fields for data collection with no interaction. The fields at which we collected data are noted by red vertical lines at 0.467, 0.633, 0.768, and 0.913 V/cm. (b) Stark map for the $37d_{5/2}$ state. Frequency scans taken with a 1 μs, 1019 nm laser pulse are overlaid with the calculated Stark lines. The frequency scan highlighted in red at 1.5 V/cm, where the different $|m_j|$ levels are well separated, was used to obtain the field ionization spectra for individual excitation of each $|m_j|$ level shown in Fig. 4.

interferometer. The second beamsplitter is provided by the LZ transition at the avoided crossing. Depending on the slew rate of the ionization ramp and the characteristics of the avoided crossing, some of the amplitude will traverse the crossing diabatically and transfer to $|1/2'\rangle$ ($|3/2'\rangle$) and some will traverse adiabatically and remain in $|1/2\rangle$ ($|3/2\rangle$) [31]. Avoided crossings do not occur between states of differing $|m_j|$ since the Stark effect does not mix them.

The two adiabatic components, $|1/2\rangle$ and $|3/2\rangle$, traverse similar paths through the Stark map until ionization where their amplitudes will combine. Because of the phase difference δt accrued during the variable delay, the signal on the detector in peak **A** will oscillate in time. Likewise, the $|1/2'\rangle$ and $|3/2'\rangle$ components will ionize together and produce peak **B** which will oscillate out of phase with peak **A**.

II. EXPERIMENT

To measure quantum beats we begin by exciting the atoms in a magneto-optical trap (MOT) to Rydberg states in a three step process. The phase of the coherent superposition is then allowed to evolve for a variable amount of time. Finally the atoms are field ionized and the time resolved signal is collected.

Our excitation takes place inside of a fairly standard vapor cell magneto-optical trap. We cool and trap roughly a million rubidium-85 atoms to a temperature of 200 μK. These atoms are situated at the center of a set of electrodes with which we can apply static and time varying electric fields. A static field is used to split the $37d_{5/2}$, $|m_j|$ states as shown in Fig. 3(b), which ultimately determines the time scale for phase evolution of the coherently excited superposition state.

Excitation of the Rydberg states is done in three steps [36]. The $5p_{3/2}$ state is populated by the trapping lasers, which are left on during the entire experimental cycle. The $5p_{3/2} \rightarrow 5d_{5/2}$ transition is driven by a 776 nm laser that we pulse on for 10 μs at a rate of 20 pulses/s. This is an external cavity diode laser locked to the electromagnetically-induced-transparency signal seen by overlapping a small portion of the 780 nm and 776 nm laser beams in a rubidium vapor cell. From the $5d_{5/2}$ state some of the atoms radiatively decay to the $6p_{3/2}$ state. At the end of the 776 nm pulse, we apply a short pulse of 1019 nm light to drive the $6p_{3/2} \rightarrow 37d_{5/2}$ transition. The 1019 nm laser is also a continuous-wave, external-cavity diode laser, but in this case we lock its frequency to an actively stabilized Fabry-Perot cavity. The 1019 nm beam is double passed through a fast, tunable acoustic-optic modulator. This allows us to tune the laser through a range of 150 MHz as well as create short pulses. The excitation volume is defined by the overlap of the perpendicular 776 nm and 1019 nm laser beams, which is located at the zero of the MOT magnetic field.

In Fig. 3(b) we show a Stark map of the $37d_{5/2}$ state. The heavy solid lines are the calculated energies of the $|m_j| = 1/2$, 3/2, and 5/2 states. Frequency scans taken with a 1 μs, 1019 nm laser pulse at a range of applied electric fields are overlaid with the calculated spectra. The width of the measured spectral lines is limited to 6 MHz

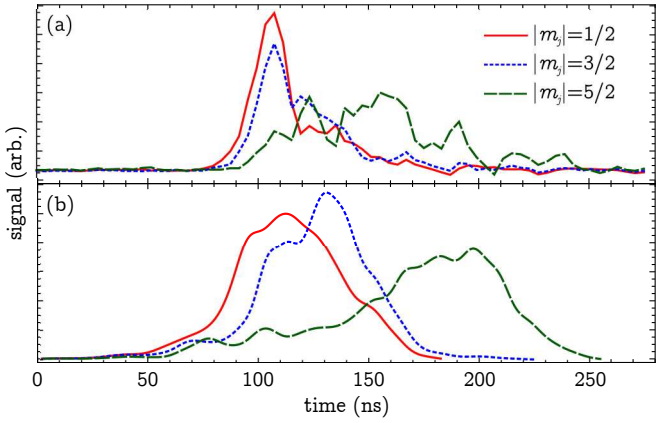

FIG. 4. (color online) Time resolved field ionization spectra for individual excitation of the $|m_j| = 1/2$, 3/2, and 5/2 states at the electric field highlighted in red near 1.5 V/cm in Fig. 3. In (a) we show the experimentally measured spectra and in (b) the calculated spectra.

by the radiative step in our excitation process. Fitting our measured spectra to this Stark map gives us a rough calibration of the field seen by the Rydberg atoms for a given set of potentials applied to the electrodes in our vacuum chamber. To more accurately calibrate the field we also collected a dipole-dipole interaction spectrum as shown in Fig. 3(a). A detailed discussion of the dipole-dipole interaction among atoms can be found in Altiere *et. al.* [37] along with the procedure used to fit to calculated interaction spectra. We estimate an uncertainty in our field calibration of 0.5%.

To excite a coherent superposition of all three $|m_j|$ states we use a 50 ns pulse of 1019 nm light with a bandwidth of 10 MHz. This allows us to excite a coherent superposition of the three states in fields of up to roughly 1 V/cm. After the Rydberg excitation pulse we wait for a variable amount of time before field ionizing the atoms. The field ionization pulse rises at a rate of ∼0.4 V/cm/ns. The time resolved signal, collected and amplified with a micro-channel plate detector, is shown in Fig. 4(a) for the case where each of the three $|m_j|$ states is excited independently using a long laser pulse (1 μs). The overlap between these three states in the field ionization signal allows them to interfere when a coherent superposition of states is excited.

III. MODEL

We calculate the Rydberg electron's path to ionization through the Stark map by iteratively time-evolving the initial state from zero electric field until ionization. While the initial states are written in the fine structure basis, as we near ionization we use hydrogen-like wave functions in the parabolic basis. The Hamiltonian for the Rydberg electron in a static electric field is

$$-\frac{1}{2}\nabla^2 + V(r) + Fz, \tag{1}$$

where $V(r)$ is the potential due to the interaction with the atomic core and Fz is the potential due to the externally applied electric field. When the Rydberg electron is in a high angular momentum state it is unlikely to penetrate the core and $V(r)$ is essentially coulombic [14]. For lower angular momentum states this is not the case and it is necessary to model the interaction using the quantum defects. We included measured quantum defects for the s, p, d, f, and g states [38–41] and we estimated the defects for higher angular momentum states based on an ℓ^{-5} scaling [42].

Following the method of Zimmerman et al. [15], we constructed the Hamiltonian matrix for the Rydberg electron in the fine structure basis $\{j, m_j\}$. Since the electron's amplitude will spread out among many states due to transitions at avoided crossings, we must include a sufficient number of states in our basis for accuracy. We tested our calculation and found that the results converged if we included ∼15-20 manifolds centered on our initial state. In the present calculation, we included states from the $n = 30$ manifold up to the $n = 47$ manifold or a basis of about 1400 states.

The electron's state at time t_i can be determined from the state at time t_{i-1} from

$$\psi(t_i) = \hat{U}(t_i)\psi(t_{i-1}) \tag{2}$$

where $\hat{U}(t_i)$ is the time evolution operator at the i^{th} time step. We can calculate $\hat{U}(t_i)$ by finding the Hamiltonian at the electric field F_i and using the shape of our field ionization ramp to map from electric field to time.

The necessary resolution in time is set by the curvature of the states at the many avoided crossings in the electron's path to ionization; a sufficient resolution in field is necessary to faithfully represent each avoided crossing. We find that in the neighborhood of the $37d$ state our results converge well for a time step of about 10^{-11} s.

Since our ramp takes our initial state to ionization in ~ 1 μs we need about 10^5 time steps. The calculation is greatly aided by the use of a supercomputer. While the time evolution must proceed serially, all of the necessary time evolution operators are calculated in parallel and stored until used.

An alternative approach would be to use Landau-Zener theory at each avoided crossing as in [32]. Many of the avoided crossings, however, involve more than two states and are not well-separated from adjacent avoided crossings. It is also much easier to preserve the phase in the present numerical method as Landau-Zener theory yields probabilities and not amplitudes.

Figure 1 shows the results of our calculation of the path to ionization for the $37d_{5/2}$ $|m_j| = 1/2$, 3/2, and 5/2 in red, blue, and green respectively. The amplitudes follow multiple branching paths to ionization [43–

45]. The opacity scale is chosen to highlight the differences between states with populations up to 0.1; states with greater population are more opaque. States with population greater than 0.1 are completely opaque. The classical ionization threshold is shown as a rough guide to the eye for where the electron ionizes. The paths to ionization for all three states clearly overlap in the neighborhood of ionization.

Our model does not include any coupling to continuum states so it will not naturally produce ionization of the electron. To estimate the ionization rate Γ as a function of F, we follow Førre and Hansen [33] and McMillian et al. [45] in using a semiempirical formula for the ionization rate of hydrogen derived by Damburg and Kolosov [46],

$$\Gamma = \frac{(4R)^{2n_2+m+1}}{n^3 n_2!(n_2+m)!} \times e^{-\frac{2}{3}R-\frac{1}{4}n^3F(34n_2^2+34n_2m+46n_2+7m^2+23m+\frac{53}{3})}, \quad (3)$$

where $R = (-2E_0)^{3/2}/F$ and n, n_2, and m are the usual parabolic quantum numbers. The energy E_0 is determined by a fourth order perturbation calculation [47]. We begin to calculate ionization rates once our calculation approaches the classical ionization threshold.

The application of Eq. (3) is motivated by the fact that the set $\{n, \ell, j, m_j\}$ cease to be good quantum numbers as the electric field increases. While the states that are well separated from the manifold (s, p, d) will retain much of their initial character until they hit the manifold, as the field increases further all Stark lines will be superpositions of many $\{n, \ell, j, m_j\}$ states. Instead, at fields near ionization, it is more natural to describe the states with parabolic quantum numbers $\{n, n_1, n_2, m\}$ [48]. A discussion of the transition from low fields, through intermediate fields, to ionization can be found in [49].

During the calculation, we have access to each Stark state as a superposition in the fine structure $\{j, m_j\}$ basis. In order to use Eq. (3) we must transform to the parabolic basis. We do this in two steps by first transforming to the spherical $\{\ell, m_\ell\}$ basis with

$$|j, m_j\rangle = \sum_{m_\ell = m_j \pm \frac{1}{2}} \langle \ell, \tfrac{1}{2}, m_\ell, m_j - m_\ell | j, m_j \rangle \, |\ell, m_\ell\rangle \,, \quad (4)$$

where the first factor on the right hand side is a Clebsch-Gordan coefficient. We then transform to the parabolic basis with

$$|n, n_1, n_2, m\rangle = \sum_\ell \langle n, \ell, m | n, n_1, n_2, m\rangle \, |n, \ell, m\rangle \,, \quad (5)$$

where the transformation coefficient is [14]

$$\langle n, \ell, m | n, n_1, n_2, m\rangle = (-1)^{1-n+m+n_1-n_2} \times \sqrt{2\ell+1} \begin{pmatrix} \frac{n-1}{2} & \frac{n-1}{2} & \ell \\ \frac{m+n_1-n_2}{2} & \frac{m-n_1+n_2}{2} & -m \end{pmatrix}. \quad (6)$$

Once in the parabolic basis, we use Eq. (3) and the size of our time step to determine an ionization probability. We use the ionization probability to remove a fraction of the amplitude from each state and we save the amplitude ionized from each parabolic state at each time step. Finally, we transform back to the fine structure $\{j, m_j\}$ basis by inverting Eqs. (4) and (5) and continue the time evolution. It is possible that the new expansion obtained upon transforming back to the $\{j, m_j\}$ basis could include states not in our original basis. In this case we would artificially lose amplitude; however, we find that this is not a significant issue given the size of our original basis.

To test our calculation, we generate field ionization spectra for each $37d_{5/2}$ $|m_j|$ sublevel individually. In this simpler case we can just calculate the probability of ionization at each time from our saved amplitudes for each $|m_j|$ state individually. Each probability is assigned a gaussian with a width based on the resolution of our detector and we sum all of the probabilities to generate an ionization spectrum. The calculated spectra shown in Fig. 4(b) are in good general agreement with the experimental spectra shown in Fig. 4(a). The time resolved signals for $|m_j| = 1/2$ and $3/2$ are almost completely overlapping, while the $|m_j| = 5/2$ signal is more spread out and peaks later in time.

One discrepancy in the calculated spectra compared to the measured spectra is in the overall width of the field ionization signals. While the calculated spectra take into account the measured shape of our field ionization pulse, they do not include the flight of the ionized electrons to the detector. In the experiment the field ionized electrons leave the region of electric field after a few centimeters of flight and then move through a field free region before arriving at the microchannel plate detector. Electrons that are ionized later in time (at higher electric field) will therefore acquire more kinetic energy as they travel in the field than the electrons ionized earlier in time (at lower electric field). This will lead to an overall compression of the electron signal at the detector. It is also worth noting that the detailed shape of the calculated results are quite sensitive to the slew rate used in the calculation, but the general features of the time resolved signals remain the same for a range of slew rates.

To calculate the full ionization spectrum including all three $|m_j|$ states, we sum the parabolic state amplitudes that ionized at each time step. The $|m_j| = 1/2$ state is a superposition of parabolic states with both $m = 0$ and $m = 1$ while the $|m_j| = 3/2$ is a superposition of parabolic states with $m = 1$ and $m = 2$. Therefore, amplitudes with a phase difference given by $(E_{1/2} - E_{3/2})t$ will combine in the $m = 1$ parabolic states, where E_{m_j} is the energy of the $37d_{5/2}, |m_j|$ sublevel at the excitation field. Similarly, the $|m_j| = 5/2$ state is a superposition of parabolic states with both $m = 2$ and $m = 3$ and so amplitudes with a phase difference given by $(E_{3/2} - E_{5/2})t$ will combine in the $m = 2$ parabolic states. The oscillations produced by this interference will sit on a back-

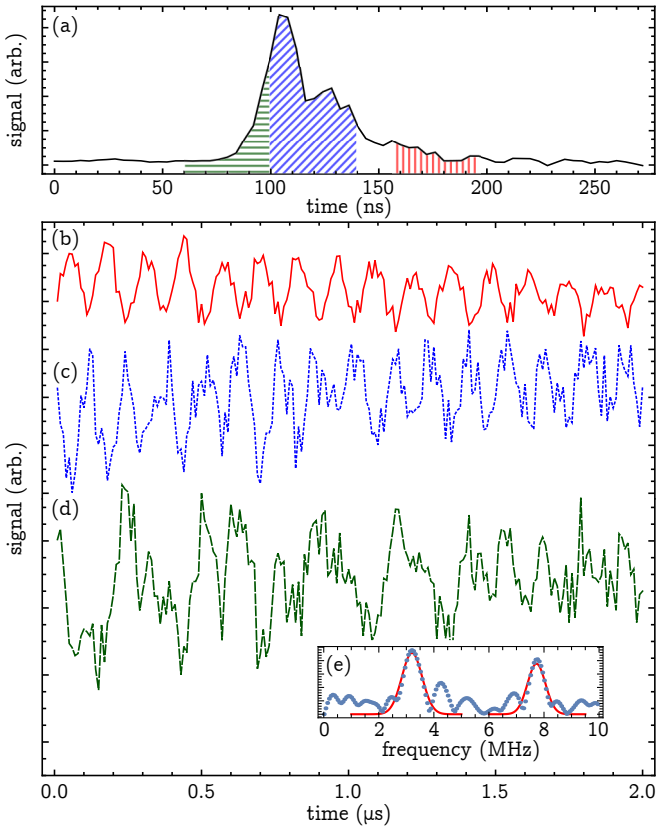

FIG. 5. (color online) Data from an electric field of 0.913 V/cm. (a) An example of the total field ionization spectrum when all three $|m_j|$ sublevels are excited with a short laser pulse. This spectrum is from a delay time of 1.0 μs. The shaded areas were integrated at each delay time from 0 to 2.0 μs and the results are plotted in (b), (c), and (d). (b) The integrated signal from the red vertically hashed gate. (c) The integrated signal from the blue diagonally hashed gate. The oscillations in (b) and (c) are clearly π out of phase. The frequency of the oscillation was determined to be 7.7±0.3 MHz from a fit to a Fourier transform peak. This matches well with the $3/2-5/2$ separation (see Table I). (d) The integrated signal from the green horizontally hashed gate. (e) Example of a Fourier spectrum used to determine the dominant frequencies in (d). Both the $1/2-3/2$ and $3/2-5/2$ frequencies are present in (d), with the lower frequency component measured to be 3.2±0.4 MHz.

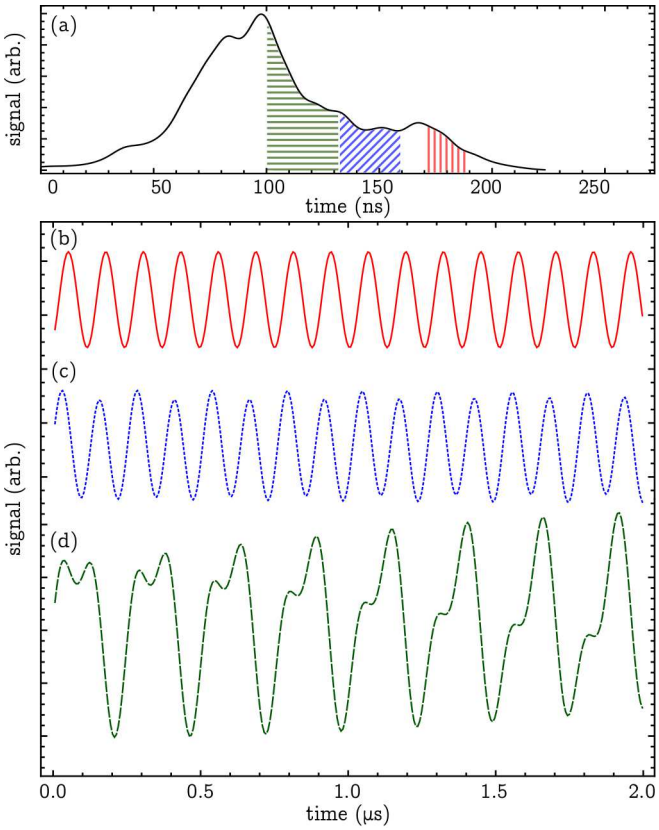

FIG. 6. (color online) Model calculated at an electric field of 0.913 V/cm. (a) An example of the total field ionization spectrum when all three $|m_j|$ sublevels combined. This spectrum is from a delay time of 1.0 μs. The shaded areas were integrated at each delay time from 0 to 2.0 μs and the results are plotted in (b), (c), and (d). (b) The integrated signal from the red vertically hashed gate. (c) The integrated signal from the blue diagonally hashed gate. The oscillations in (b) and (c) are out of phase by approximately $\pi/2$. If we compare to Fig. 5(b) and (c), where these oscillations are π out of phase, it is clear that our model is missing some relevant phase evolution. (d) The integrated signal from the green horizontally hashed gate. This gate was chosen for comparison to to Fig. 5(d), since both the $1/2-3/2$ and $3/2-5/2$ frequencies are present.

ground of $m=0$ and $m=3$ parabolic states not involved in any interference.

IV. RESULTS AND DISCUSSION

We collected quantum beat data at the four fields marked in Fig. 3. At each field we scanned the time delay between excitation and ionization over a range of 0 to 2 μs in 10 ns steps. We then gated the time resolved electron signal over several different regions to reveal quantum beats that result from interference among the different pathways that ionize at a particular field.

Figure 5 shows a representative set of data taken at a field of 0.913 V/cm. In Fig. 5(a) we see the time resolved field ionization signal at one particular time delay along with the three gates used in (b)-(d). Clear oscillations are seen in the gated data. Figure 5(b) oscillates at a frequency corresponding to the $|m_j|=3/2$ to 5/2 separation at this field. Figure 5(c) oscillates at this frequency as well, but is out of phase with the oscillations in (b). In effect, the interference has directed a portion of the electron wave function to split and ionize at one field or the other depending on the relative phase accumulated between the $|m_j|=3/2$ and 5/2 states. In Fig. 5(d) we see oscillations at two frequencies, one corresponding to the $|m_j|=3/2$ to 5/2 separation and the other to the

TABLE I. Comparison of measured to calculated oscillation frequencies. The measured frequencies were determined by fitting the peaks in a Fourier spectrum. The error in the measurement is from both the width of those peaks and the uncertainty in the field calibration.

	$1/2-3/2$		$3/2-5/2$	
field (V/cm)	calc. (MHz)	fit (MHz)	calc. (MHz)	fit (MHz)
0.467	1.02	0.7±0.4	2.05	2.0±0.3
0.633	1.86	1.4±0.3	3.77	3.7±0.3
0.768	2.73	2.2±0.4	5.56	5.4±0.3
0.913	3.85	3.2±0.4	7.87	7.7±0.3

$|m_j| = 1/2$ to $3/2$ separation. It is worth noting that the total population, that is the total integrated field ionization signal, remains constant over all time delays.

The oscillation frequencies were found by Fourier transforming the time dependent data. The Fourier spectrum for the data in Fig. 5(d) is shown in the inset labeled (e). Oscillation frequencies for the four fields at which we measured quantum beats are summarized in Table I. There is generally good agreement between the measured and calculated frequencies, although some of the oscillations at the $|m_j| = 1/2$ to $3/2$ separation fall outside of our error estimates. Our error estimates come from two sources. First, the resolution of our Fourier spectra is limited to 0.3 MHz due to the finite measurement time of 2 μs. The second error is derived from our error in the field calibration leading to a frequency error of 0.1 MHz. These two errors are combined in quadrature resulting in the the values quoted in Table I. Likely sources of error include the inhomogeneity of the applied electric field and the MOT magnetic field across the excitation volume.

Fig. 6 shows the result of the calculation for the same field of 0.913 V/cm as in Fig. 5. Since the calculated and measured spectra in Fig. 4 do not entirely match, it is not possible to use the same integration gates as in Fig. 5(a). In Fig. 6(b) and (c) oscillations are seen corresponding to the $|m_j| = 3/2$ to $5/2$ separation at this field. The oscillations are not π out of phase as in Fig. 5(b) and (c), rather they are about $\pi/2$ out of phase. Fig. 6(d) shows an oscillation from a gate in which two frequencies, one corresponding to the $|m_j| = 3/2$ to $5/2$ separation and the other to the $|m_j| = 1/2$ to $3/2$ separation, are present; this is similar to Fig. 5(d). None of the oscillations in Fig. 6 show any decline in amplitude as we do not include any sources of dephasing in our model.

The fact that the relative phase of the oscillations in Fig. 6(b) and (c) does not agree with the corresponding plots in Fig. 5 is an indication that our model does not capture all relevant phase information. This is likely due to the way in which our model handles the time evolution near ionization. Our basis does not include any continuum states; rather, we discretely remove amplitude based on Eq (3). As the electron nears ionization it will evolve into a superposition involving continuum states and the phase evolution is likely to be different than in our model.

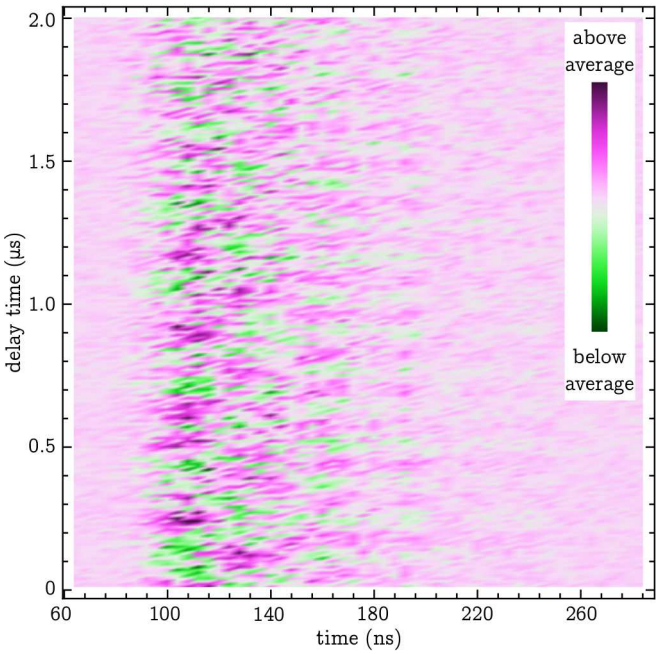

FIG. 7. (color online) Image showing the time resolved field ionization spectrum at each time delay. The vertical axis displays the delay time between Rydberg excitation and field ionization. On the horizontal axis is the arrival time of the electrons at the detector relative to the start of the field ionization pulse plus a constant fixed offset. The fixed offset is chosen so that the time resolved electron signal begins near the start of our oscilloscope trace. This allows us to achieve good time resolution with fewer samples. Triggering relative to the start of the field ionization pulse also keeps the time resolved signal from shifting as the delay time between the excitation and field ionization pulses is increased. The average signal is subtracted from each trace to enhance the visibility of the oscillations. The amplitude of the signal is given by the color scale shown in the legend.

Given the rich information contained in this data set, we also present it as an image, which shows the complete field ionization spectrum at each time delay. Since the visibility of the oscillations is rather low, we have averaged the field ionization signal over all time delays and subtracted this average from each delay to produce the image shown in Fig. 7.

V. CONCLUSION

We have observed quantum beats in the field ionization of a coherent superposition of Rydberg states. While

the data presented here is for the $37d_{5/2}$ states, we have observed quantum beats for a variety of nd states ranging from $n = 28$ to 46 as well as a variety of $np_{3/2}$ states. We have also developed a model of the ionization pathway through the complex Stark map to ionization.

Our observation of quantum beats as well as our ability to accurately model the field ionization process has paved the way to more interesting quantum control experiments. Tailoring the shape of the field ionization pulse so that it moves more quickly, more slowly, or multiple times through each of the avoided crossings should allow us to direct the electron to ionize at the desired field. One goal might be to design a field ionization pulse that can separate the signal from two states that would be unresolvable with the typical ramped field ionization pulse. Given the large number of avoided crossings that a Rydberg state encounters on its path to ionization, designing a pulse by hand that produces the desired result would be a daunting task. We therefore plan to use a genetic algorithm to optimize the ionization pathway.

This work was based upon work supported by the National Science Foundation under Grant No. 0653544.

This work used the Extreme Science and Engineering Discovery Environment (XSEDE), which is supported by National Science Foundation grant number OCI-1053575.

[1] Jonathon A. Sedlacek, Arne Schwettmann, Harald Kubler, Robert Low, Tilman Pfau, and James P. Shaffer, "Microwave electrometry with Rydberg atoms in a vapour cell using bright atomic resonances," Nat Phys **8**, 819–824 (2012).

[2] J. A. Sedlacek, A. Schwettmann, H. Kübler, and J. P. Shaffer, "Atom-based vector microwave electrometry using rubidium Rydberg atoms in a vapor cell," Phys. Rev. Lett. **111**, 063001 (2013).

[3] S. B. Hill, C. B. Haich, Z. Zhou, P. Nordlander, and F. B. Dunning, "Ionization of xenon Rydberg atoms at a metal surface," Phys. Rev. Lett. **85**, 5444–5447 (2000).

[4] J. D. Carter, O. Cherry, and J. D. D. Martin, "Electric-field sensing near the surface microstructure of an atom chip using cold Rydberg atoms," Phys. Rev. A **86**, 053401 (2012).

[5] R. R. Jones, D. You, and P. H. Bucksbaum, "Ionization of Rydberg atoms by subpicosecond half-cycle electromagnetic pulses," Phys. Rev. Lett. **70**, 1236–1239 (1993).

[6] Sha Li and R. R. Jones, "Ionization of excited atoms by intense single-cycle THz pulses," Phys. Rev. Lett. **112**, 143006 (2014).

[7] R. C. Stoneman, D. S. Thomson, and T. F. Gallagher, "Microwave multiphoton transitions between Rydberg states of potassium," Phys. Rev. A **37**, 1527–1540 (1988).

[8] K. A. H. van Leeuwen, G. v. Oppen, S. Renwick, J. B. Bowlin, P. M. Koch, R. V. Jensen, O. Rath, D. Richards, and J. G. Leopold, "Microwave ionization of hydrogen atoms: Experiment versus classical dynamics," Phys. Rev. Lett. **55**, 2231–2234 (1985).

[9] Michael W. Noel, W. M. Griffith, and T. F. Gallagher, "Classical subharmonic resonances in microwave ionization of lithium Rydberg atoms," Phys. Rev. A **62**, 063401 (2000).

[10] Michael W. Noel, W. M. Griffith, and T. F. Gallagher, "Population trapping in extremely highly excited states in microwave ionization," Phys. Rev. Lett. **83**, 1747–1750 (1999).

[11] W. Zhao, J. J. Mestayer, J. C. Lancaster, F. B. Dunning, C. O. Reinhold, S. Yoshida, and J. Burgdörfer, "Bidirectionally kicked Rydberg atoms: Population trapping near the continuum," Phys. Rev. A **73**, 015401 (2006).

[12] Michael W. Noel, Lung Ko, and T. F. Gallagher, "Microwave ionization of an atomic electron wave packet," Phys. Rev. Lett. **87**, 043001 (2001).

[13] K. R. Overstreet, R. R. Jones, and T. F. Gallagher, "Phase-dependent energy transfer in a microwave field," Phys. Rev. A **85**, 055401 (2012).

[14] Thomas F. Gallagher, *Rydberg Atoms*, Cambridge Monographs on Atomic, Molecular, and Chemical Physics (Cambridge University Press, 1994).

[15] Myron L. Zimmerman, Michael G. Littman, Michael M. Kash, and Daniel Kleppner, "Stark structure of the Rydberg states of alkali-metal atoms," Phys. Rev. A **20**, 2251–2275 (1979).

[16] Clarence Zener, "Non-adiabatic crossing of energy levels," Proc. R. Soc. Lond. A **137**, 696–702 (1932).

[17] Lev D Landau, "Zur theorie der energieubertragung. II," Physics of the Soviet Union **2**, 28 (1932).

[18] E. C. G. Stückelberg, "Theorie der unelastischen stösse zwischen atomen," Helvetica Physica Acta **5**, 369 (1932).

[19] Ettore Majorana, "Atomi orientati in campo magnetico variabile," Il Nuovo Cimento (1924-1942) **9**, 43–50 (1932).

[20] William D. Oliver, Yang Yu, Janice C. Lee, Karl K. Berggren, Leonid S. Levitov, and Terry P. Orlando, "Mach-Zehnder interferometry in a strongly driven superconducting qubit," Science **310**, 1653 (2005).

[21] Guozhu Sun, Xueda Wen, Bo Mao, Jian Chen, Yang Yu, Peiheng Wu, and Siyuan Han, "Tunable quantum beam splitters for coherent manipulation of a solid-state tripartite qubit system," Nat Commun **1**, 51 (2010).

[22] J. R. Petta, H. Lu, and A. C. Gossard, "A coherent beam splitter for electronic spin states," Science **327**, 669 (2010).

[23] G. D. Fuchs, G. Burkard, P. V. Klimov, and D. D. Awschalom, "A quantum memory intrinsic to single nitrogen-vacancy centres in diamond," Nat Phys **7**, 789–793 (2011).

[24] Xinsheng Tan, Dan-Wei Zhang, Zhentao Zhang, Yang Yu, Siyuan Han, and Shi-Liang Zhu, "Demonstration of geometric Landau-Zener interferometry in a superconducting qubit," Phys. Rev. Lett. **112**, 027001 (2014).

[25] C. W. S. Conover, M. C. Doogue, and F. J. Struwe, "Chirped-pulse multiphoton transitions between Rydberg states," Phys. Rev. A **65**, 033414 (2002).

[26] J. Lambert, Michael W. Noel, and T. F. Gallagher, "Rydberg-atom population transfer by population trapping in a chirped microwave pulse," Phys. Rev. A **66**, 053413 (2002).

[27] H. Maeda, J. H. Gurian, and T. F. Gallagher, "Population transfer by multiphoton adiabatic rapid passage," Phys. Rev. A **83**, 033416 (2011).

[28] Nicolas Saquet, Anne Cournol, Jérôme Beugnon, Jacques Robert, Pierre Pillet, and Nicolas Vanhaecke, "Landau-Zener transitions in frozen pairs of Rydberg atoms," Phys. Rev. Lett. **104**, 133003 (2010).

[29] M Tada, Y Kishimoto, M Shibata, K Kominato, S Yamada, T Haseyama, I Ogawa, H Funahashi, K Yamamoto, and S Matsuki, "Manipulating ionization path in a Stark map: Stringent schemes for the selective field ionization in highly excited Rb Rydberg," Physics Letters A **303**, 285 – 291 (2002).

[30] A. Gürtler and W.J. van der Zande, "ℓ-state selective field ionization of rubidium Rydberg states," Physics Letters A **324**, 315 – 320 (2004).

[31] Jan R. Rubbmark, Michael M. Kash, Michael G. Littman, and Daniel Kleppner, "Dynamical effects at avoided level crossings: A study of the Landau-Zener effect using Rydberg atoms," Phys. Rev. A **23**, 3107–3117 (1981).

[32] F. Robicheaux, C. Wesdorp, and L. D. Noordam, "Selective field ionization in Li and Rb: Theory and experiment," Phys. Rev. A **62**, 043404 (2000).

[33] M. Førre and J. P. Hansen, "Selective-field-ionization dynamics of a lithium $m = 2$ Rydberg state: Landau-Zener model versus quantal approach," Phys. Rev. A **67**, 053402 (2003).

[34] G. Leuchs and H. Walther, "Quantum interference effects in field ionization: Application to the measurement of the fine structure splitting of highly excited Na^2D states," Z. Physik A **293**, 93–101 (1979).

[35] T. H. Jeys, K. A. Smith, F. B. Dunning, and R. F. Stebbings, "Investigation of fine-structure quantum beats in sodium rydberg atoms by field ionization," Phys. Rev. A **23**, 3065–3070 (1981).

[36] Donald P. Fahey and Michael W. Noel, "Excitation of Rydberg states in rubidium with near infrared diode lasers," Opt. Express **19**, 17002–17012 (2011).

[37] Emily Altiere, Donald P. Fahey, Michael W. Noel, Rachel J. Smith, and Thomas J. Carroll, "Dipole-dipole interaction between rubidium Rydberg atoms," Phys. Rev. A **84**, 053431 (2011).

[38] Wenhui Li, I. Mourachko, M. W. Noel, and T. F. Gallagher, "Millimeter-wave spectroscopy of cold Rb Rydberg atoms in a magneto-optical trap: Quantum defects of the ns , np , and nd series," Phys. Rev. A **67**, 052502 (2003).

[39] Jianing Han, Yasir Jamil, D. V. L. Norum, Paul J. Tanner, and T. F. Gallagher, "Rb nf quantum defects from millimeter-wave spectroscopy of cold ^{85}Rb Rydberg atoms," Phys. Rev. A **74**, 054502 (2006).

[40] K. Afrousheh, P. Bohlouli-Zanjani, J. A. Petrus, and J. D. D. Martin, "Determination of the ^{85}Rb ng-series quantum defect by electric-field-induced resonant energy transfer between cold Rydberg atoms," Phys. Rev. A **74**, 062712 (2006).

[41] B. Sanguinetti, H. O. Majeed, M. L. Jones, and B. T. H. Varcoe, "Precision measurements of quantum defects in the $n\mathrm{P}_{3/2}$ Rydberg states of 85^{Rb}," J. Phys. B: At. Mol. Opt. Phys. **42**, 165004 (2009).

[42] Richard R. Freeman and Daniel Kleppner, "Core polarization and quantum defects in high-angular-momentum states of alkali atoms," Phys. Rev. A **14**, 1614–1619 (1976).

[43] T. H. Jeys, G. W. Foltz, K. A. Smith, E. J. Beiting, F. G. Kellert, F. B. Dunning, and R. F. Stebbings, "Diabatic field ionization of highly excited sodium atoms," Phys. Rev. Lett. **44**, 390–393 (1980).

[44] J L Vialle and H T Duong, "Field ionisation study of high lying rydberg states of na," Journal of Physics B: Atomic and Molecular Physics **12**, 1407 (1979).

[45] G B McMillian, T H Jeys, K A Smith, F B Dunning, and R F Stebbings, "High-resolution field ionisation of na(ns, nd) rydberg atoms," Journal of Physics B: Atomic and Molecular Physics **15**, 2131 (1982).

[46] R J Damburg and V V Kolosov, "A hydrogen atom in a uniform electric field. III," Journal of Physics B: Atomic and Molecular Physics **12**, 2637 (1979).

[47] Harris J. Silverstone, "Perturbation theory of the Stark effect in hydrogen to arbitrarily high order," Phys. Rev. A **18**, 1853–1864 (1978).

[48] H.A. Bethe and E.E. Salpeter, *Quantum mechanics of one- and two-electron atoms* (Springer, 1957).

[49] T. H. Jeys, G. B. McMillian, K. A. Smith, F. B. Dunning, and R. F. Stebbings, "Electric field ionization of highly excited sodium nd atoms," Phys. Rev. A **26**, 335–340 (1982).